Summary of the 2021/2022 Asian Winter Monsoon

This report summarizes the characteristics of the surface climate and atmospheric/oceanographic conditions related to the Asian winter monsoon for 2021/2022.

Note: The Japanese 55-year Reanalysis dataset (JRA-55; Kobayashi et al. 2015) and COBE-SST (Ishii et al. 2005) were used to analyze atmospheric circulation and sea surface temperature (SST). NOAA Interpolated Outgoing Longwave Radiation (OLR) data (Liebmann and Smith 1996) from the U.S. NOAA Physical Sciences Laboratory (PSL) (https://psl.noaa.gov/data/gridded/data.interp_OLR.html) were used to infer tropical convective activity. The base period for the normal is 1991 to 2020. The term "anomaly" as used in this report refers to deviation from the normal.

1. Surface climate conditions

In winter 2021/2022, three-month (DJF) mean temperatures were above normal in and around Central Asia and below normal over southwestern China and western Japan (Figure 3-1 (a)). Above-normal temperatures over parts of Eastern Siberia and below-normal temperatures over western Japan were seen in January and February (Figure 3-1 (c–d)), in contrast to the temperature anomaly observed in December (Figure 3-1 (b)). Temperatures were significantly below normal over most of East Asia in February (Figure 3-1 (d)), corresponding to a stronger-than-normal East Asian Winter Monsoon (EAWM). Precipitation amounts during the winter period were above normal over a wide region from South Asia to southwestern China and the southeastern part of Eastern Siberia, and were below normal from the Korean Peninsula to western Japan (Figure 3-2). Above-normal precipitation over a wide region of Southeast Asia was clearly seen in February in particular (Figure 3-2 (d)).

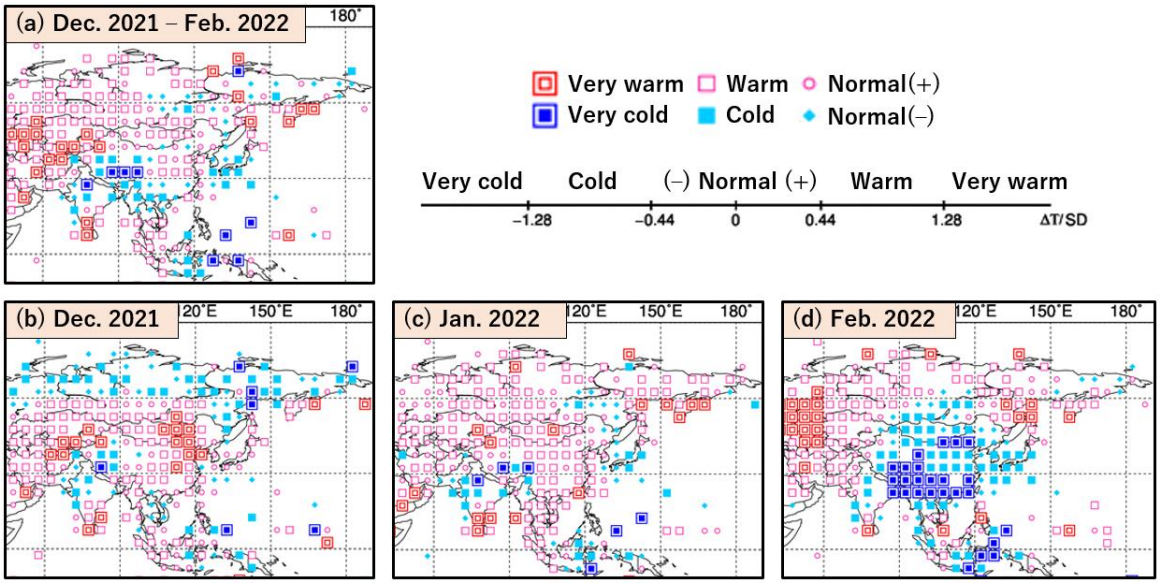

Figure 3-1 Temperature anomalies for (a) December 2021 to February 2022, (b) December 2021, (c) January 2022 and (d) February 2022

Categories are defined by the three-month/monthly mean temperature anomaly against the normal divided by its standard deviation and averaged in 5° × 5° grid boxes. The thresholds of each category are –1.28, –0.44, 0, +0.44 and +1.28. Standard deviations were calculated from 1991 – 2020 statistics. Areas over land without graphical marks are those where observation data are insufficient or where normal data are unavailable.

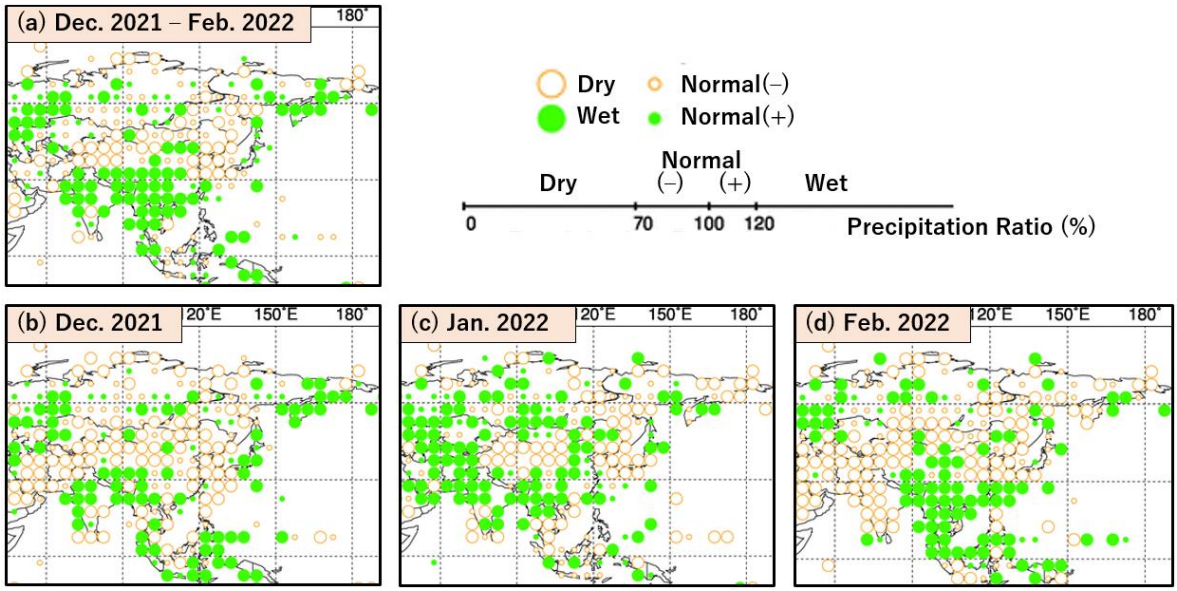

Figure 3-2 Precipitation ratio for (a) December 2021 to February 2022, (b) December 2021, (c) January 2022 and (d) February 2022

Categories are defined by the three-month/monthly precipitation ratio against the normal and averaged in 5° × 5° grid boxes. The thresholds of each category are 70, 100 and 120%. Areas over land without graphical marks are those where observation data are insufficient or where normal data are unavailable.

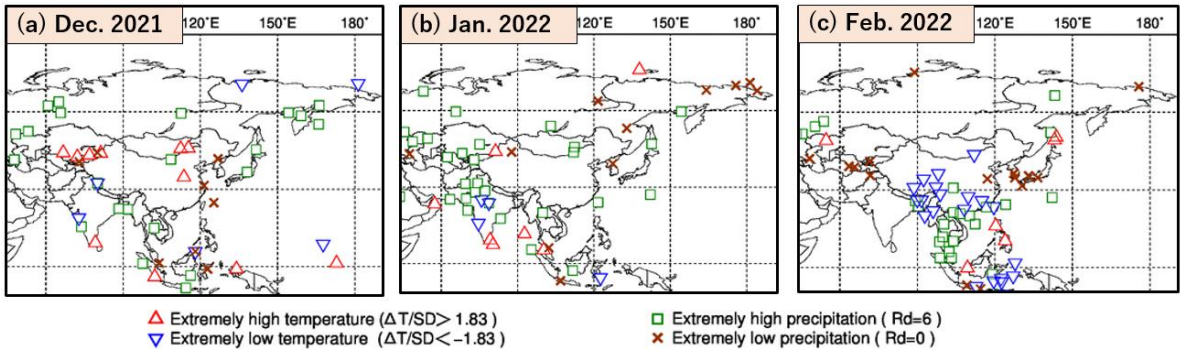

Figure 3-3 Extreme climate stations for (a) December 2021, (b) January 2022 and (c) February 2022

ΔT, SD and Rd indicate temperature anomaly, standard deviation and quintile, respectively.

Figure 3-3 plots stations where extreme climate conditions were observed during the period from December 2021 to February 2022. Extremely low temperatures were seen in and around southern China in February (Figure 3-3 (c); see also Figure 3-1 (d)). Extremely high precipitation amounts were seen in and around northwestern India in January (Figure 3-3 (b)) and on and around the Indochina Peninsula in February (Figure 3-3 (c)). Extremely low precipitation amounts were seen in and around western Japan in February (Figure 3-3 (c)).

2. Characteristic atmospheric circulation and oceanographic conditions

This section presents characteristics of atmospheric circulation and oceanographic conditions averaged for winter 2021/2022.

2.1 Conditions in the tropics

Figure 3-4 shows three-month mean SST anomalies and anomalous convective activity seen during the winter period. SSTs exhibited negative anomalies east of 170°E in the equatorial Pacific and positive anomalies over the tropical western North Pacific (Figure 3-4 (a)) in association with the La Niña event that persisted from boreal autumn 2021 onward. In the Indian Ocean, remarkably positive SST anomalies were seen in the Bay of Bengal and west of Sumatra (Figure 3-4 (a)). Convective activity inferred from OLR was enhanced from the Philippines to the seas north of New Guinea and suppressed from near the date line to the central part of the equatorial Pacific (Figure 3-4 (b)), corresponding to SST anomalies associated with the La Niña event (Figure 3-4 (a)). In the upper troposphere, large-scale divergence anomalies were dominant near the Maritime Continent, and large-scale convergence anomalies were seen from the date line to the east over the equatorial Pacific, concomitant with tropical convection (Figure 3-4 (b)). Large-scale anomalous divergence promoted northward divergent winds from the Maritime Continent to the seas south of Japan (vectors in Figure 3-4 (b)), partly contributing to a meandering of the subtropical jet stream (STJ) as described later.

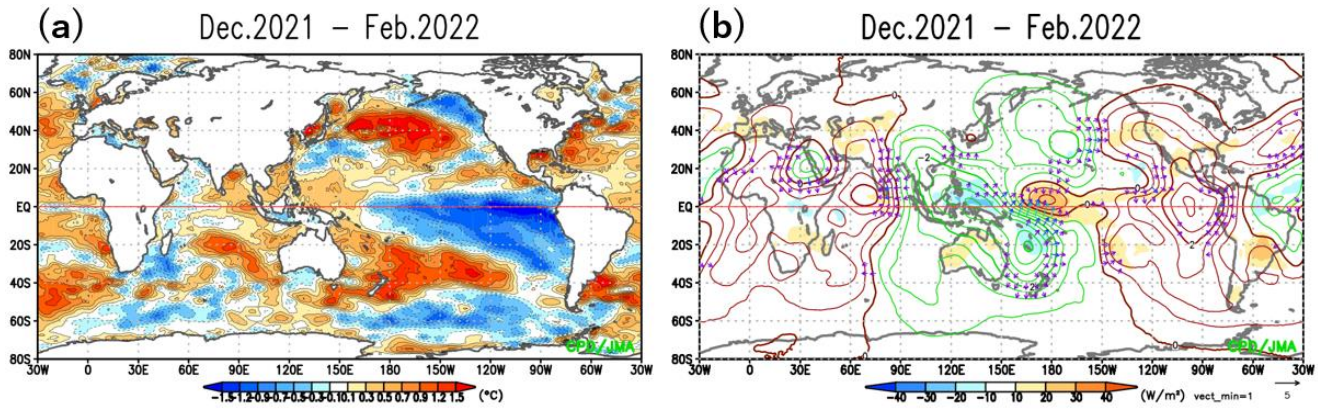

Figure 3-4 Three-month mean (a) SST anomalies and (b) anomalous convective activity in winter 2021/2022

Shading in (a) and (b) shows SST anomalies [°C] and OLR anomalies [W/m^2]. Contours and vectors in (b) indicate 200-hPa velocity potential anomalies at intervals of 0.5 × 10^6 m^2/s and divergent wind anomalies, respectively. Negative (cold color) and positive (warm color) OLR anomalies show enhanced and suppressed convective activity compared to the normal, respectively.

Figure 3-5 shows three-month mean 200-hPa and 850-hPa stream function anomalies for the winter period. In the upper troposphere, a Rossby wave train was dominant along the STJ from the eastern part of Northern Africa to the seas east of Japan. The wave train was associated with anti-cyclonic circulation anomalies over the East China Sea and cyclonic circulation anomalies near western China and to the east of Japan (Figure 3-5 (a)). The cyclonic circulation anomalies near western China, which imply a southward meandering of the STJ, correspond to below-normal temperatures and above-normal precipitation near southwestern China (Figures 3-1 (a) and 3-2 (a)). The anti-cyclonic circulation anomalies over the East China Sea may have been partly caused by northward divergent winds from the Maritime Continent, where enhanced convection was seen (Figure 3-4 (b)). This is also supported by vorticity budget analysis and the results of a numerical experiment conducted using a linear baroclinic model (Watanabe and Kimoto 2000, 2001) (not shown). In the central tropical Pacific, cyclonic circulation anomalies straddling the equator were seen in response to suppressed convection from near the date line to the eastern part of the equatorial Pacific (Figure 3-5 (a)). A great circle wave train was clearly seen from the central tropical North Pacific via North America to the North Atlantic, which is similar to behavior seen in the negative phase of the Pacific-North American (PNA) teleconnection pattern (e.g., Barnston and Livezey 1987, Horel and Wallace 1981). In the lower troposphere, anti-

cyclonic circulation anomalies straddling the equator were seen from the central to eastern tropical Pacific in response to suppressed convection from near the date line to the eastern part of the equatorial Pacific (Figure 3-5 (b)).

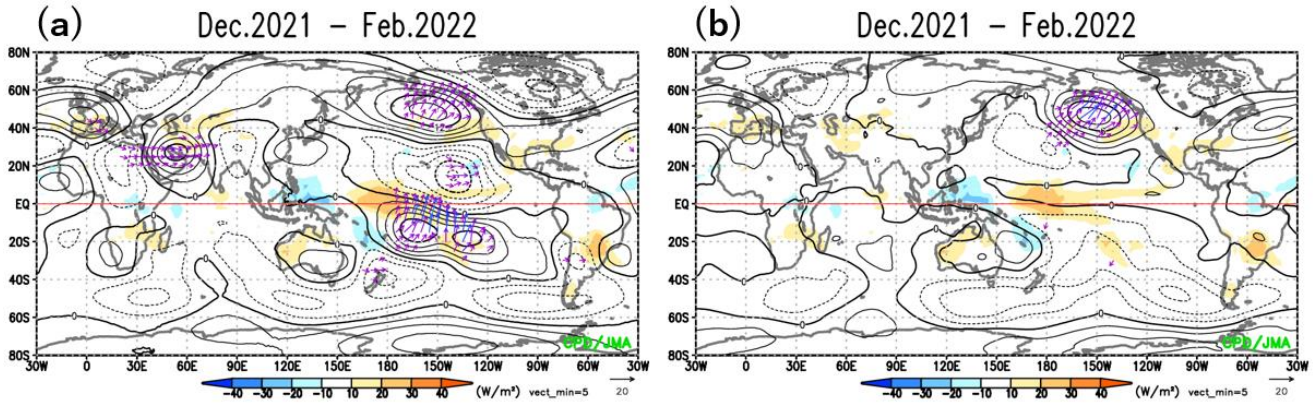

Figure 3-5 Three-month mean (a) 200-hPa and (b) 850-hPa stream function anomalies in winter 2021/2022

Contours indicate stream function anomalies at intervals of (a) 3×10^6 m^2/s and (b) 1.5×10^6 m^2/s, and shading shows OLR anomalies [W/m^2]. Vectors denote horizontal components of wave activity flux [m^2/s^2] as defined by Takaya and Nakamura (2001).

2.2 Conditions in the extratropics

Figure 3-6 shows three-month mean 500-hPa height, sea level pressure and 850-hPa temperature in the Northern Hemisphere. In the 500-hPa height field (Figure 3-6 (a)), significant positive anomalies were seen over Eastern Siberia, implying significantly frequent blocking-high formation over the region (figure not shown), and negative anomalies were seen to the south. The north-south dipole pattern of the height anomalies resembles the Western Pacific (WP) teleconnection pattern (Wallace and Gutzler 1981). The tropospheric polar vortex in the Northern Hemisphere centered from the Arctic region to northern Canada was stronger than normal. Part of the enhanced polar vortex split and moved southward to just north of Japan (contours in Figure 3-6 (a)). Wave trains associated with height anomalies were seen from Eurasia to Japan along the polar-front jet (PFJ) over northern Eurasia and the STJ over southern Eurasia. Another wave train in the Western Hemisphere from the mid-latitude North Pacific to the western North Atlantic corresponded to the negative phase of the PNA pattern (see also Figure 3-5 (a)). In the sea level pressure field (Figure 3-6 (b)), the Aleutian Low was stronger than normal and shifted southwestward from its normal position. Positive SLP anomalies from Eastern Siberia to China indicate a stronger-than-normal Siberian High. The pattern of SLP anomalies indicates a stronger-than-normal EAWM, corresponding to below-normal temperatures from southern China to mainland Japan in the lower troposphere (Figure 3-6 (c)). Lower-level temperatures, by contrast, were above normal over Siberia in association with positive 500-hPa height anomalies (Figure 3-6 (a)).

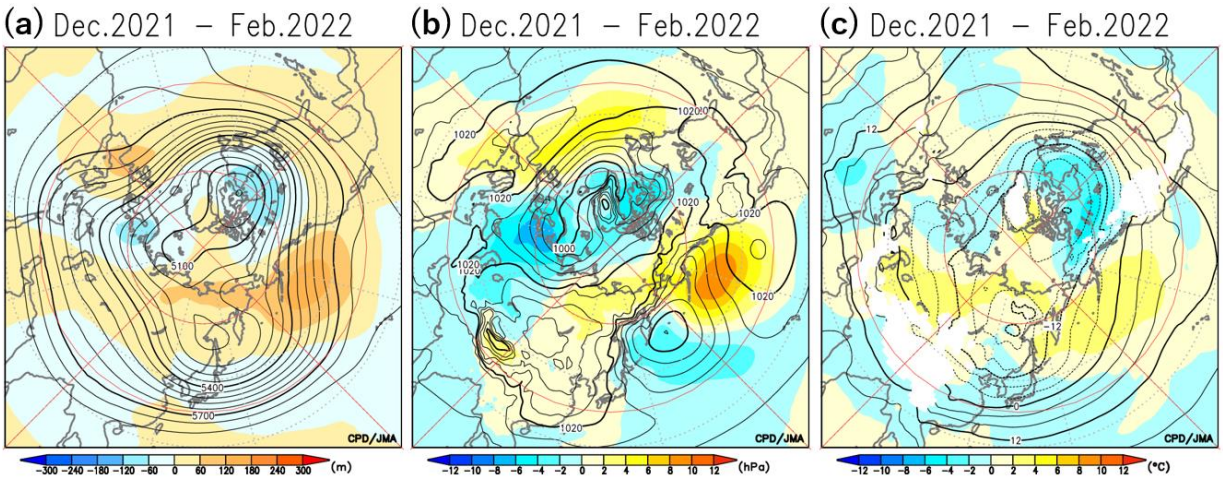

Figure 3-6 Three-month mean (a) 500-hPa height, (b) sea level pressure and (c) 850-hPa temperature in winter 2021/2022
Contour intervals are (a) 60 m, (b) 4 hPa and (c) 4 °C. Shading denotes related anomalies.

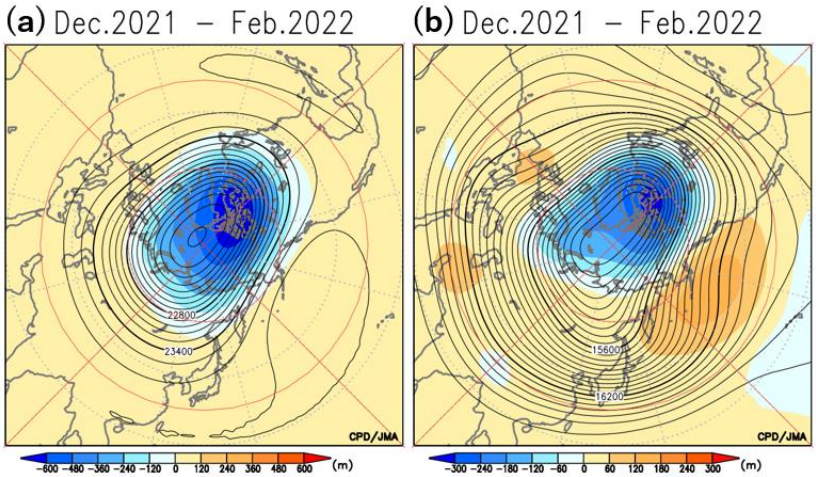

Figure 3-7 Three-month mean (a) 30-hPa and (b) 100-hPa height in winter 2021/2022
Contour intervals are (a) 120 m and (b) 60 m. Shading denotes related anomalies.

In the sea level pressure field, significant negative and positive anomalies with a north-south dipole pattern were seen over the North Atlantic, showing the positive phase of the North-Atlantic Oscillation (NAO; e.g., Hurrell 1995). The NAO in winter is known to be associated with stratospheric circulation caused by stratosphere-troposphere interaction (e.g., Ambaum and Hoskins 2002, Ineson and Scaife 2009). Figure 3-7 shows three-month mean 30-hPa and 100-hPa height in the Northern Hemisphere. Negative height anomalies at 30 hPa and 100 hPa were clearly seen from the Arctic region to northern Canada, indicating that the stratospheric polar vortex was stronger than normal and slightly shifted toward Canada during the winter period. The negative anomalies seen over northern Canada in the stratosphere correspond well with those seen in the troposphere (Figure 3-6 (a)) and near the surface (Figure 3-6 (b)), suggesting a close relationship to the positive phase of the NAO resulting from stratosphere–troposphere interaction.

(Kazuto Takemura, Tokyo Climate Center)

References

Ambaum, M. H. P., and B. J. Hoskins, 2002: The NAO troposphere–stratosphere connection. *J. Climate*, **15**, 1969–1978.

Barnston, A. G., and R. E. Livezey, 1987: Classification, seasonality and persistence of low-frequency atmospheric circulation patterns. *Mon. Wea. Rev.*, **115**, 1083–1126.

Horel, J. D., and J. M. Wallace, 1981: Planetary-scale atmospheric phenomena associated with the Southern Oscillation. *Mon. Wea. Rev.*, **109**, 813–829.

Hurrell, J. W., 1995: Decadal trends in the North Atlantic Oscillation and relationships to regional temperature and precipitation. *Science*, **269**, 676–679.

Ineson, S., and I. I. Scaife, 2009: The role of the stratosphere in the European climate response to El Niño. *Nature Geosci.*, **2**, 32–36.

Ishii, M., A. Shouji, S. Sugimoto, and T. Matsumoto, 2005: Objective analyses of sea-surface temperature and marine meteorological variables for the 20th century using ICOADS and the Kobe Collection. *Int. J. Climatol.*, **25**, 865–879.

Kobayashi, S., Y. Ota, Y. Harada, A. Ebita, M. Moriya, H. Onoda, K. Onogi, H. Kamahori, C. Kobayashi, H. Endo, K. Miyaoka, and K. Takahashi, 2015: The JRA-55 Reanalysis: General specifications and basic characteristics. *J. Meteor. Soc. Japan*, **93**, 5–48.

Liebmann, B., and C. A. Smith, 1996: Description of a complete (interpolated) outgoing longwave radiation dataset. *Bull. Amer. Meteor. Soc.*, **77**, 1275–1277.

Takaya, K., and H. Nakamura, 2001: A formulation of a phase-independent wave-activity flux for stationary and migratory quasigeostrophic eddies on a zonally varying basic flow, *J. Atom. Sci.*, **58**, 608–627.

Wallace, J, M., and D. S. Gutzler, 1981: Teleconnections in the geopotential height field during the Northern Hemisphere winter, *Mon. Wea. Rev.*, **109**, 784–812.

Watanabe, M., and M. Kimoto, 2000: Atmospheric-ocean thermal coupling in the North Atlantic: A positive feedback. *Quart. J. Roy. Meteor. Soc.*, **126**, 3343–3369.

Watanabe, M., and M. Kimoto, 2001: Corrigendum. *Quart. J. Roy. Meteor. Soc.*, **127**, 733–734.

<<Table of contents <Top of this article